International Journal of Heat and Fluid Flow 29 (2008) 1326–1336

Contents lists available at ScienceDirect

International Journal of Heat and Fluid Flow

journal homepage: www.elsevier.com/locate/ijhff

Numerical study of natural convection in partially heated rectangular enclosures filled with nanofluids

Hakan F. Oztop [a], Eiyad Abu-Nada [b,*]

[a] Department of Mechanical Engineering, Firat University, Elazig TR-23119, Turkey
[b] Department of Mechanical Engineering, Hashemite University, Zarqa 13115, Jordan

ARTICLE INFO

Article history:
Received 8 January 2008
Received in revised form 22 April 2008
Accepted 28 April 2008
Available online 18 June 2008

Keywords:
Nanofluids
Heat transfer
Natural convection
Enclosure

ABSTRACT

Heat transfer and fluid flow due to buoyancy forces in a partially heated enclosure using nanofluids is carried out using different types of nanoparticles. The flush mounted heater is located to the left vertical wall with a finite length. The temperature of the right vertical wall is lower than that of heater while other walls are insulated. The finite volume technique is used to solve the governing equations. Calculations were performed for Rayleigh number ($10^3 \leqslant Ra \leqslant 5 \times 10^5$), height of heater ($0.1 \leqslant h \leqslant 0.75$), location of heater ($0.25 \leqslant y_p \leqslant 0.75$), aspect ratio ($0.5 \leqslant A \leqslant 2$) and volume fraction of nanoparticles ($0 \leqslant \varphi \leqslant 0.2$). Different types of nanoparticles were tested. An increase in mean Nusselt number was found with the volume fraction of nanoparticles for the whole range of Rayleigh number. Heat transfer also increases with increasing of height of heater. It was found that the heater location affects the flow and temperature fields when using nanofluids. It was found that the heat transfer enhancement, using nanofluids, is more pronounced at low aspect ratio than at high aspect ratio.

1. Introduction

Buoyancy induced flow and heat transfer is an important phenomenon in engineering systems due to its wide applications in electronic cooling, heat exchangers, double pane windows etc. These applications are reviewed by Ostrach (1988). Enhancement of heat transfer in these systems is an essential topic from an energy saving perspective. The low thermal conductivity of convectional heat transfer fluids such as water and oils is a primary limitation in enhancing the performance and the compactness of such systems. An innovative technique to improve heat transfer is by using nano-scale particles in the base fluid (Choi, 1995).

Nanotechnology has been widely used in industry since materials with sizes of nanometers possess unique physical and chemical properties. Nano-scale particle added fluids are called as nanofluid which is firstly utilized by Choi (1995). Some numerical and experimental studies on nanofluids include thermal conductivity (Kang et al. 2006), convective heat transfer (Maiga et al, 2005; Abu-Nada, 2008), boiling heat transfer and natural convection (Xuan and Li, 2000). Detailed review studies are published by Putra et al. (2003), Wang et al. (2006), Xuan and Li (2000), Trisaksri and Wongwises (2007), Daungthongsuk and Wongwises (2007), and Wang and Mujumdar (2007).

Studies on natural convection using nanofluids are very limited and they are related with differentially heated enclosures. Hwang et al. (2007) investigated the buoyancy-driven heat transfer of water-based Al_2O_3 nanofluids in a rectangular cavity. They showed that the ratio of heat transfer coefficient of nanofluids to that of base fluid is decreased as the size of nanoparticles increases, or the average temperature of nanofluids is decreased. Khanafer et al. (2003) investigated the heat transfer enhancement in a two-dimensional enclosure utilizing nanofluids for various pertinent parameters. They tested different models for nanofluid density, viscosity, and thermal expansion coefficients. It was found that the suspended nanoparticles substantially increase the heat transfer rate any given Grashof number. Jou and Tzeng (2006) used nanofluids to enhance natural convection heat transfer in a rectangular enclosure. They conducted a numerical study using Khanafer's model. They indicated that volume fraction of nanofluids cause an increase in the average heat transfer coefficient. Jang and Choi (2004) investigated the Benard regime in nanofluid filled rectangular enclosures. Wang et al. (2006) conducted a study on natural convection in nanofluid filled vertical and horizontal enclosures. Also, a recent study by Polidori et al. (2007) analyzed the heat transfer enhancement in natural convection using nanofluids.

Natural convection heat transfer in a partially heated enclosure is an important issue due to wide applications in buildings or cooling of flush mounted electronic heaters. Chu et al. (1976) conducted an experimental and numerical study to analyze the effects

* Corresponding author. Tel.: +962 390 3333; fax: +962 382 6613.
E-mail address: eiyad@hu.edu.jo (E. Abu-Nada).

0142-727X/$ - see front matter © 2008 Elsevier Inc. All rights reserved.
doi:10.1016/j.ijheatfluidflow.2008.04.009

Nomenclature

A	aspect ratio (W/H)
C_p	specific heat at constant pressure (kJ kg^{-1} K^{-1})
g	gravitational acceleration (m s^{-2})
H	height of the enclosure (m)
h	local heat transfer coefficient (W m^{-2} K^{-1})
h	dimensionless length of partial heater, h'/H
h'	length of heater, (m)
k	thermal conductivity (W m^{-1} K^{-1})
Nu	Nusselt number, $Nu = hH/k$
Nu_{avg}	average Nusselt number
Pr	Prandtl number
q_w	heat flux, (W m^{-2})
Ra	Rayleigh number
T	dimensional temperature (K)
u, v	dimensional x and v components of velocity (m s^{-1})
U, V	dimensionless x and v components of velocity
W	length of the enclosure (m)
x, y	dimensionless coordinates
y_p	dimensionless center of heater
y'_p	center of location of heater (m)

Greek symbols

α	fluid thermal diffusivity (m^2 s^{-1})
β	thermal expansion coefficient (K^{-1})
ε	numerical tolerance
φ	nanoparticle volume fraction
ϕ	transport quantity
ν	kinematic viscosity (m^2 s^{-1})
θ	dimensionless temperature
Ψ	dimensionless stream function
ψ	dimensional stream function (m^2 s^{-1})
Ω	dimensionless vorticity
ω	dimensional vorticity (s^{-1})
ρ	density (kg m^{-3})
μ	dynamic viscosity (N s m^{-2})

Subscripts

avg	average
nf	nanofluid
f	fluid
H	hot
L	cold
s	solid
w	wall
p	particle

of heater size, location, aspect ratio and boundary conditions on natural convection in a rectangular air filled enclosure. They indicated that heater size and location are important parameters on flow and temperature field and heat transfer. The problem of temperature and flow field in a partially heated enclosure for different conditions in air or water filled enclosure has been studied extensively in the last three decades (Farouk and Fusegi, 1989; Koca et al. 2007; Varol et al., 2006; Ishihara et al. 2002; Nasr et al. 2006; Aydin and Yang, 2000; Turkoglu and Yucel, 1995; Ahmed and Yovanovich, 1992; Hasnaoui et al., 1992; Chao et al., 1983).

The main aim of this study is to examine the natural convection heat transfer in a partially heated rectangular enclosure filled with nanofluids. Three different nanofluids as Cu, Al_2O_3 and TiO_2 are tested to investigate the effect of nanoparticles on natural convection flow and temperature fields. The mentioned literature survey indicates that there is no study on natural convection in a partially heated enclosure filled with nanofluid.

2. Governing equations and problem formulation

Fig. 1 shows a schematic diagram of the partially heated enclosure. The fluid in the enclosure is a water based nanofluid containing different type of nanoparticles: Cu, Al_2O_3, and TiO_2. The nanofluid is assumed incompressible and the flow is assumed to be laminar. It is assumed that the base fluid (i.e. water) and the nanoparticles are in thermal equilibrium and no slip occurs between them. The thermo physical properties of the nanofluid are given in Table 1. The left wall is maintained at a constant temperature (T_H) higher than the right wall (T_L). The thermo-physical properties of the nanofluid are assumed to be constant except for the density variation, which is approximated by the Boussinesq model.

The governing equations for the laminar and steady state natural convection in terms of the stream function-vorticity formulation are

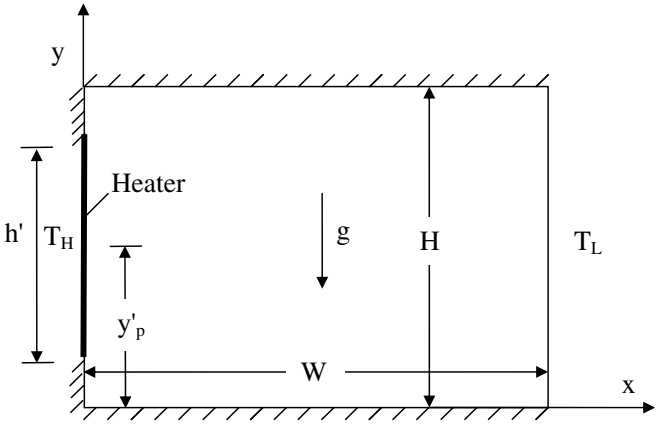

Fig. 1. Sketch of problem geometry and coordinates.

Vorticity

$$\frac{\partial}{\partial x'}\left(\omega\frac{\partial\psi}{\partial y'}\right)-\frac{\partial}{\partial y'}\left(\omega\frac{\partial\psi}{\partial x'}\right)=\frac{\mu_{nf}}{\rho_{nf}}\left(\frac{\partial\omega}{\partial x'^2}+\frac{\partial\omega}{\partial y'^2}\right)+\frac{(\varphi\rho_s\beta_s+(1-\varphi)\rho_f\beta_f)}{\rho_{nf}}g\left(\frac{\partial T}{\partial x'}\right) \quad (1)$$

Energy

$$\frac{\partial}{\partial x'}\left(T\frac{\partial\psi}{\partial y'}\right)-\frac{\partial}{\partial y'}\left(T\frac{\partial\psi}{\partial x'}\right)=\frac{\partial}{\partial x'}\left[\alpha_{nf}\frac{\partial T}{\partial x'}\right]+\frac{\partial}{\partial y'}\left[\alpha_{nf}\frac{\partial T}{\partial y'}\right] \quad (2)$$

Kinematics

$$\frac{\partial^2\psi}{\partial x'^2}+\frac{\partial^2\psi}{\partial y'^2}=-\omega \quad (3)$$

$$\alpha_{nf}=\frac{k_{eff}}{(\rho c_p)_{nf}} \quad (4)$$

The effective density of the nanofluid is given as

$$\rho_{nf} = (1-\varphi)\rho_f + \varphi\rho_s \tag{5}$$

The heat capacitance of the nanofluid is expressed as (Abu-Nadu, 2007; Khanafer et al. (2003)):

$$(\rho c_p)_{nf} = (1-\varphi)(\rho c_p)_f + \varphi(\rho c_p)_s \tag{6}$$

The effective thermal conductivity of the nanofluid is approximated by the Maxwell–Garnetts model

$$\frac{k_{nf}}{k_f} = \frac{k_s + 2k_f - 2\varphi(k_f - k_s)}{k_s + 2k_f + \varphi(k_f - k_s)} \tag{7}$$

The use of this equation is restricted to spherical nanoparticles where it does not account for other shapes of nanoparticles. This model is found to be appropriate for studying heat transfer enhancement using nanofluids (Akbarinia and Behzadmehr, 2007; Abu-Nada, 2008; Palm et al., 2006; Maiga et al., 2005) .The viscosity of the nanofluid can be approximated as viscosity of a base fluid μ_f containing dilute suspension of fine spherical particles and is given by Brinkman (1952):

$$\mu_{nf} = \frac{\mu_f}{(1-\varphi)^{2.5}} \tag{8}$$

The radial and tangential velocities are given by the following relations respectively,

$$u = \frac{\partial\psi}{\partial y'}, \tag{9}$$

$$v = -\frac{\partial\psi}{\partial x'}. \tag{10}$$

The following dimensionless groups are introduced

$$x = \frac{x'}{H};\quad y = \frac{y'}{H};\frac{\Omega}{=}\frac{\omega H^2}{\alpha_f};\quad \Psi = \frac{\psi}{\alpha_f};\quad V = \frac{vH}{\alpha_f};$$
$$U = \frac{uH}{\alpha_f};\quad \theta = \frac{T - T_L}{T_H - T_L}. \tag{11}$$

By using the dimensionless parameters the equations are written as

$$\frac{\partial}{\partial x}\left(\Omega\frac{\partial\Psi}{\partial y}\right) - \frac{\partial}{\partial y}\left(\Omega\frac{\partial\Psi}{\partial x}\right) = \left[\frac{Pr}{(1-\varphi)^{0.25}\left((1-\varphi)+\varphi\frac{\rho_s}{\rho_f}\right)}\right]\left(\frac{\partial\Omega}{\partial x^2}+\frac{\partial\Omega}{\partial y^2}\right)$$
$$+ RaPr\left[\frac{1}{\frac{(1-\varphi)}{\varphi}\frac{\rho_f}{\rho_s}+1}\frac{\beta_s}{\beta_f}+\frac{1}{\frac{\varphi}{(1-\varphi)}\frac{\rho_f}{\rho_s}+1}\right]\left(\frac{\partial T}{\partial x}\right) \tag{12}$$

$$\frac{\partial}{\partial x}\left(\theta\frac{\partial\Psi}{\partial y}\right) - \frac{\partial}{\partial y}\left(\theta\frac{\partial\Psi}{\partial x}\right) = \frac{\partial}{\partial x}\left(\lambda\frac{\partial\theta}{\partial x}\right) + \frac{\partial}{\partial y}\left(\lambda\frac{\partial\theta}{\partial y}\right) \tag{13}$$

$$\frac{\partial^2\Psi}{\partial x^2} + \frac{\partial^2\Psi}{\partial y^2} = -\Omega \tag{14}$$

$$\lambda = \frac{\frac{k_{nf}}{k_f}}{(1-\varphi)+\varphi\frac{(\rho c_p)_s}{(\rho c_p)_f}} \tag{15}$$

$$Ra = \frac{g\beta H^3(T_H - T_L)}{v\alpha} \tag{16}$$

The dimensionless radial and tangential velocities are given as, respectively:

$$U = \frac{\partial\Psi}{\partial y}, \tag{17}$$

$$V = -\frac{\partial\Psi}{\partial x}. \tag{18}$$

The dimensionless boundary conditions are written as

$$\left.\begin{array}{l} 1 - \text{On the left wall(heater)i.e.,} x = 0, \Psi = 0, \Omega = -\frac{\partial^2\Psi}{\partial x^2}, \theta = 1. \\ 2 - \text{On the left wall(no heater)i.e.,} x = 0, \Psi = 0, \Omega = -\frac{\partial^2\Psi}{\partial x^2}, \frac{\partial\theta}{\partial x} = 0. \\ 3 - \text{On the right wall i.e.,} x = 1, \Psi = 0, \Omega = -\frac{\partial^2\Psi}{\partial x^2}, \theta = 0. \\ 4 - \text{On the top and bottom walls} : \Psi = 0, \Omega = -\frac{\partial^2\Psi}{\partial y^2}, \frac{\partial\theta}{\partial y} = 0. \end{array}\right\} \tag{19}$$

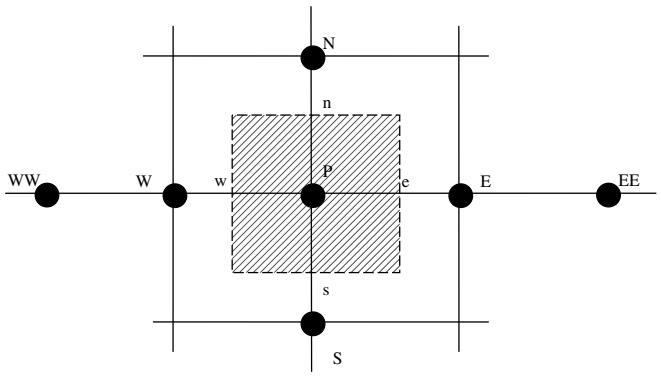

Fig. 2. Typical control volume.

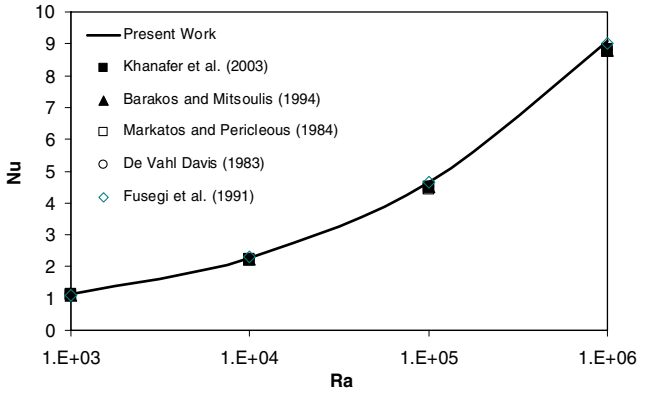

Fig. 3. Nusselt number versus *Ra* number and comparison with other published works. (See above-mentioned references for further information.)

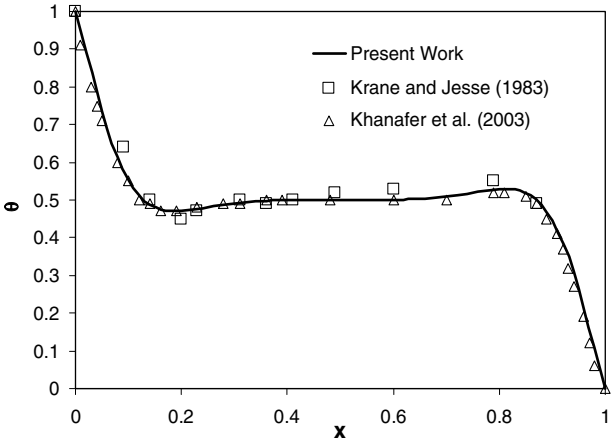

Fig. 4. Comparison between present work and other published data for the temperature distribution on the left wall ($Ra = 10^5$, $Pr = 0.7$).

3. Numerical implementation

Eqs. (12)–(14) with corresponding boundary conditions given in Eq. (19) are solved using the finite volume approach (Patankar (1980), Versteeg and Malalasekera (1995)). The diffusion term in the vorticity and energy equations is approximated by a second-order central difference scheme which gives a stable solution. Furthermore, a second order upwind differencing scheme is adopted for the convective terms. The algebraic finite volume equations for the vorticity and energy equations are written into the following form:

$$a_P\phi_P = a_E\phi_E + a_W\phi_W + a_N\phi_N + a_S\phi_S + b \tag{20}$$

where P, W, E, N, S denote cell location, west face of the control volume, east face of the control volume, north face of the control volume and south face of the control volume respectively (see Fig. 2). Similar expression is also used for the kinematics equation where only central difference is used for the discritization at the cell P of the control volume. The resulted algebraic equations are solved using successive over/under relaxation method. Successive under relaxation was used due to the non-linear nature of the governing equations especially for the vorticity equation at high Rayleigh numbers. The convergence criterion is defined by the following expression:

$$\varepsilon = \frac{\sum_{j=1}^{j=M}\sum_{i=1}^{i=N}|\phi^{n+1} - \phi^{n}|}{\sum_{j=1}^{j=M}\sum_{i=1}^{i=N}|\phi^{n+1}|} < 10^{-6} \tag{21}$$

where ε is the tolerance; M and N are the number of grid points in the x and y directions, respectively.

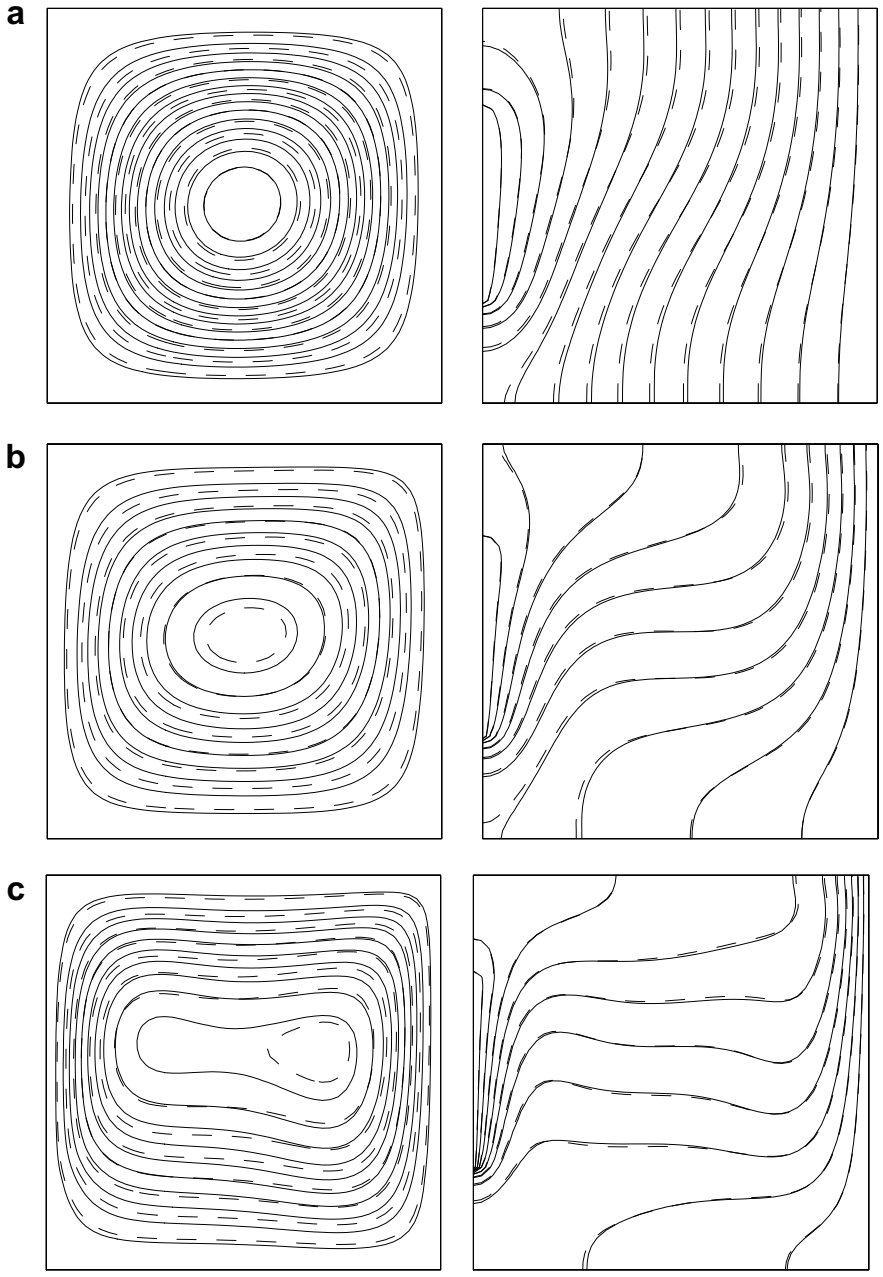

Fig. 5. Streamlines (on the left) and Isotherms (on the right) for Cu-water nanofluids (---), pure fluid (—), $h = 0.5$, $A = 1$, $y_p = 0.5$, $\varphi = 0.1$, (a) $Ra = 10^4$, (b) $Ra = 10^5$, (c) $Ra = 5 \times 105$.

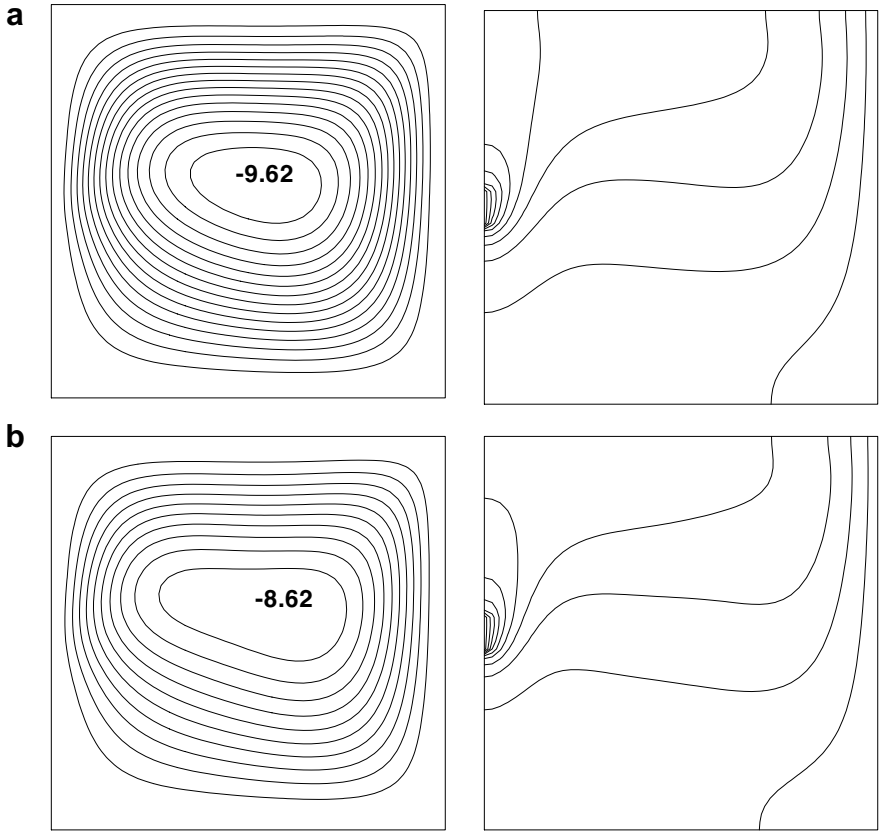

Fig. 6. Streamlines (on the left) and isotherms (on the right) for Cu-water nanofluids, $Ra = 10^5$, $y_p = 0.5$, $A = 1$, $h = 0.1$, (a) $\varphi = 0.2$, (b) $\varphi = 0.1$.

An accurate representation of vorticity at the surface is the most critical step in the stream function vorticity formulation. A second order accurate formula is used for the vorticity boundary condition. For example, the vorticity at the bottom wall is expressed as:

$$\Omega = -\frac{(8\Psi_{1,j} - \Psi_{2,j})}{2(\Delta y)^2} \tag{22}$$

Similar expressions are written for other walls. After solving Ψ, Ω, and T, further useful quantities are obtained. For example, the Nusselt number can be expressed as

$$Nu = \frac{hH}{k_f} \tag{23}$$

The heat transfer coefficient is expressed as

$$h = \frac{q_w}{T_H - T_L} \tag{24}$$

The thermal conductivity is expressed as

$$k_{nf} = -\frac{q_w}{\partial T/\partial x} \tag{25}$$

By substituting Eqs. (24), (25), and (7) into Eq. (23), and using the dimensionless quantities, the Nusselt number on the left wall is written as:

$$Nu = -\left(\frac{k_{nf}}{k_f}\right)\frac{\partial T}{\partial x} \tag{26}$$

The average Nusselt number is defined as

$$Nu_{avg} = \int_0^1 Nu(y)\mathrm{d}y \tag{27}$$

A 1/3rd Simpson's rule of integration is used to evaluate Eq. (27).

4. Grid testing and code validation

An extensive mesh testing procedure was conducted to guarantee a grid independent solution. Seven different mesh combinations were used for the case of $Ra = 10^5$ and $Pr = 0.7$. The present code was tested for grid independence by calculating the average Nusselt number on the left wall. It is found that a grid size of 51×51 ensures a grid independent solution. The converged value ($Nu = 4.644$) was compared to other known values reported by other researchers as shown in Fig. 3. Therefore, the converged value compares very well with other values obtained in literature.

The present numerical solution is further validated by comparing the present code results for $Ra = 10^5$ and $Pr = 0.70$ against the experiment of Krane and Jessee (1983) and numerical simulation of Khanafer et al. (2003). It is clear that the present code is in good agreement with other work reported in literature as shown in Fig. 4.

5. Results and discussion

Numerical analysis of buoyancy induced flow in a partially heated rectangular enclosure filled with nanofluid has been performed using the MG model. The effect of volume fraction of nanofluid, aspect ratio, type of nanoparticles, length of the heater, location of the heater and Rayleigh number are analyzed. The base case was taken as $A = 1$ (square cavity), $Ra = 10^5$, $h = 0.5$, $y_p = 0.5$ and $\varphi = 0.1$. Prandtl number is taken as $Pr = 6.2$.

Fig. 5(a)–(c) shows a comparison between Cu-water nanofluid (plotted by dashed lines) and pure fluid (plotted by solid lines) on streamlines (on the left) and isotherms (on the right) using different values of Rayleigh number. The figure demonstrates that a single circulation cell is formed in the clockwise direction for all

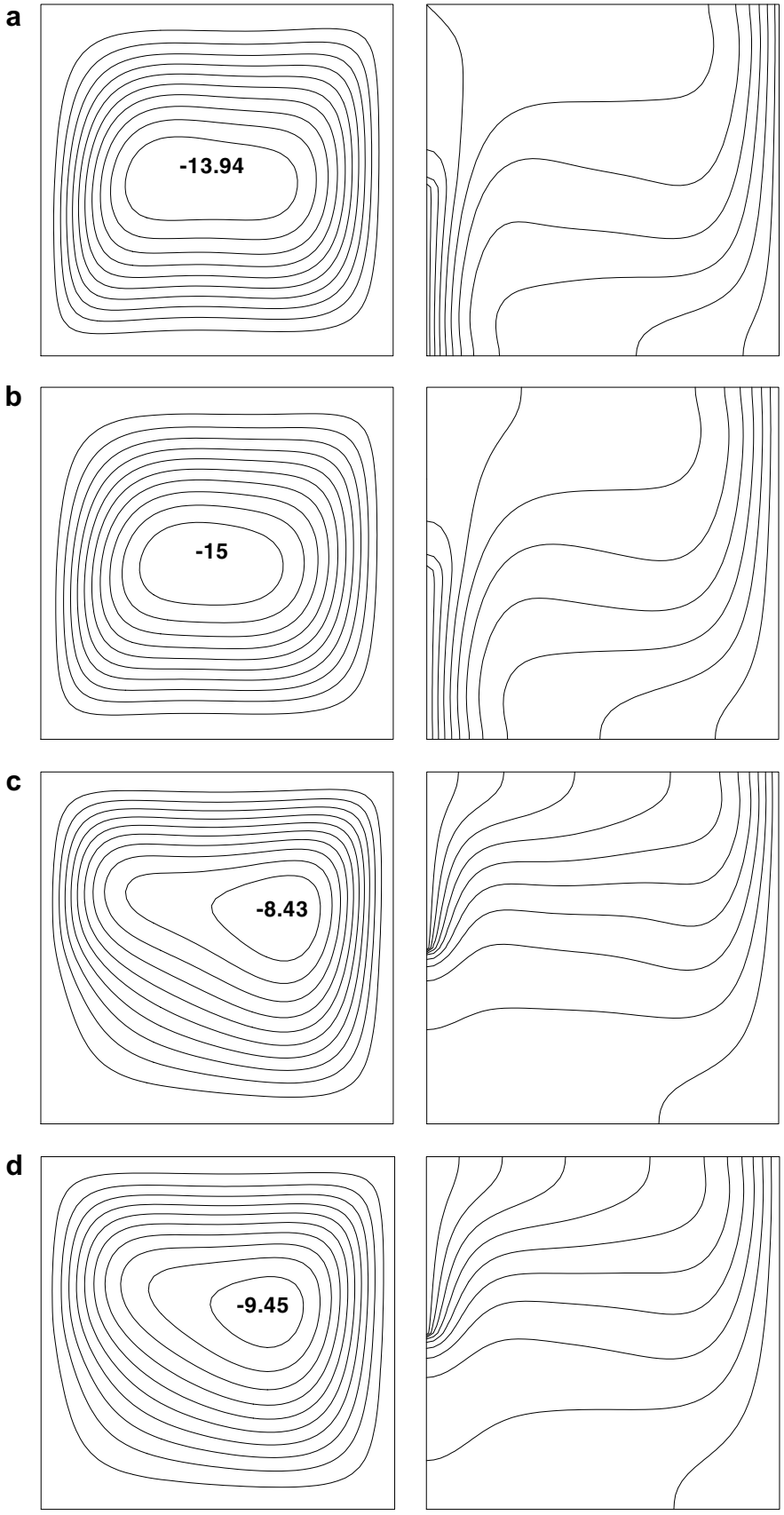

Fig. 7. Streamlines (on the left) and isotherms (on the right) for $Ra = 10^5$, $h = 0.5$, $A = 1$, (a) $\varphi = 0.1$, $y_p = 0.25$, (b) $\varphi = 0.2$, $y_p = 0.25$, (c) $\varphi = 0.1$, $y_p = 0.75$, (d) $\varphi = 0.2$, $y_p = 0.75$.

values of Rayleigh numbers. Fig. 5(a) presents the case of $Ra = 10^4$ where a circular shaped cell is formed with $\psi_{min} = -4.84$. The corresponding isotherms exhibit the characteristics of conduction dominated regime since they are distributed approximately paral-

lel to the vertical walls. As the Rayleigh number increases, the length cell increases and egg shaped cell is observed as shown in Fig. 5(b). By increasing the value of Rayleigh number the flow strength increases and the boundary layers become more distinguished. Isotherms show that temperature gradients near the heater and cold wall become more severe. For $Ra = 5 \times 10^5$, the streamlines elongate parallel to the horizontal wall for pure fluid. Also, an oval shaped circulation cell was observed near the right vertical wall as seen from Fig. 5(c).

Volume fraction of nanoparticles is a key parameter for studying the effect of nanoparticles on flow fields and temperature distributions. Thus, Fig. 6(a) and (b) are prepared to present the effect of volume fraction of nanoparticles. The figure includes streamlines (on the left) and isotherms (on the right) for $Ra = 10^5$, $y_p = 0.5$, $h = 0.1$. As shown from the figure, an egg shaped circulation cell is formed for the case of $\varphi = 0.2$ with $\psi = -9.62$. However, it moves towards to the heater for $\varphi = 0.1$. The comparison indicates that more fluid is heated for higher values of volume fraction of nanoparticles as shown from the isotherms. Flow strength also increases with increasing of volume fraction of nanoparticles.

Fig. 7 is presented to show the effects of both heater location and volume fraction of nanoparticles on flow fields and temperature distribution. Fig. 7(a) illustrates the streamline (on the left) and isotherm (on the right) for $\varphi = 0.1$, $h = 0.5$ and $y_p = 0.25$. For this case, oval shaped circulation cell is formed with $\psi_{min} = -13.94$ due to cavity heated from the bottom corner. When volume fraction of nanoparticles increases from 0.1 to 0.2, length of the circulation cell becomes smaller and flow strength increases, as seen from Fig. 7(b). When the heater is placed on the upper half part of the enclosure, i.e., $y_p = 0.75$, an egg-shaped recirculation cell is observed with $\psi_{min} = -8.43$ for $\varphi = 0.1$ (Fig. 7(c)) and $\psi_{min} = -9.45$ for $\varphi = 0.2$ (Fig. 7(d)). When the heater is located in the upper half, the flow strength decreases compared with the location in the lower half. This is due to impingement of hot fluid to the top insulated wall. In this case, the fluid at right bottom corner becomes motionless due to impingement of circulated fluid to the middle of the left vertical wall. Also, the half bottom of the cavity becomes cooler than the upper half part. Overall observation of Fig. 7 shows that as the volume fraction increases, movements of particles become irregular and random due to increasing of energy exchange rates in the fluid.

Table 1
Thermophysical properties of fluid and nanoparticles

Physical properties	Fluid phase (water)	Cu	Al_2O_3	TiO_3
C_p(J/kgK)	4179	385	765	686.2
ρ (kg/m^3)	997.1	8933	3970	4250
K (W/mK)	0.613	400	40	8.9538
$\alpha \times 10^7$ (m^2/s)	1.47	1163.1	131.7	30.7
$\beta \times 10^{-5}$ (1/K)	21	1.67	0.85	0.9

Fig. 8 compares the streamlines and isotherms using different nano-fluids as TiO_2-water and Al_2O_3-water and using different Rayleigh number as $Ra = 10^4$ (Fig. 8(a)) and $Ra = 10^5$ (Fig. 8(b)). For both nanofluids, a single circulation cell was observed in the clockwise directions. For lower values of Rayleigh number, the flow strength is higher for Al_2O_3 than that of TiO_2. On the contrary, the flow strength becomes smaller for Al_2O_3 at $Ra = 10^5$. Isotherms show almost same distribution for these two nanofluids due to closer value of thermal conductivity of Al_2O_3 and TiO_2 which is given in Table 1.

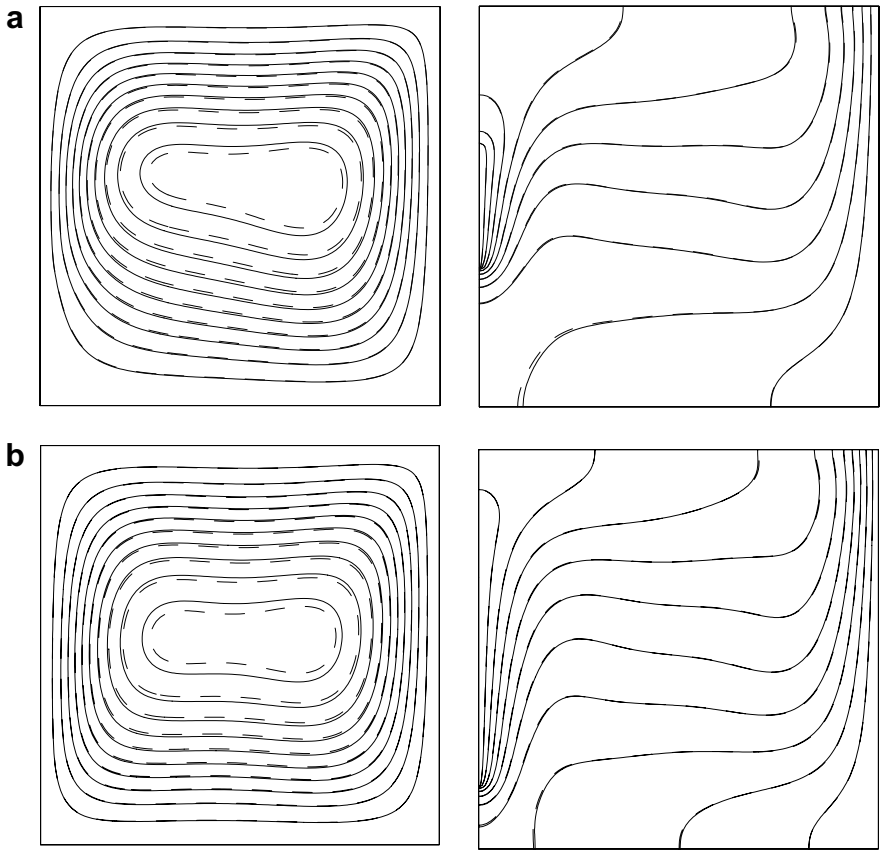

Fig. 8. Streamlines (on the left) and isotherms (on the right) $h = 0.5$, $A = 1$, $y_p = 0.25$ (a) $Ra = 10^4$, (b) $Ra = 10^5$ (----) TiO_2 ($\psi_{min} = -5.391$ for $Ra = 10^4$ and $\psi_{min} = -19.18$ for $Ra = 10^5$), Al_2O_3 (—), ($\psi_{min} = -8.387$ for $Ra = 10^4$ and $\psi_{min} = -14.23$ for $Ra = 10^5$).

Fig. 9 shows the streamlines and isotherms using different aspect ratios. It is clear that the flow strength and the temperature isotherms are influenced by the presence of nanoparticles. The behavior is similar to the trend encountered at $A = 1$.

Fig. 10(a)–(c) presents the variation of mean Nusselt number with volume fraction using different nanoparticles and different values of Rayleigh number. Results are presented for the base case, i.e., $h = 0.5$ and $y_p = 0.5$. The figure shows that the heat transfer increases almost monotonically with increasing the volume fraction for all Rayleigh numbers and nanofluids. For $Ra = 10^3$ (Fig. 9(a)), the lowest heat transfer was obtained for TiO_2 due to domination of conduction mode of heat transfer since TiO_2 has the lowest value of thermal conductivity compared to Cu and Al_2O_3. However, the difference in the values of Al_2O_3 and Cu is negligible. The thermal conductivity of Al_2O_3 is approximately one tenth of Cu, as given in Table 1. However, a unique property of Al_2O_3 is its low thermal diffusivity, Table 1. The reduced value of thermal diffusivity leads to higher temperature gradients and, therefore, higher enhancements in heat transfer. The Cu nanoparticles have high values of thermal diffusivity and, therefore, this reduces temperature gradients which will affect the performance of Cu nanoparticles. As volume fraction of nanoparticles increases, difference for mean Nusselt number becomes larger especially at higher Rayleigh numbers due to increasing of domination of convection mode of heat transfer. The highest heat transfer is recorded when using Cu-nanofluids for $\varphi = 0.2$ and $Ra = 10^5$.

Fig. 11 presents the vertical velocity profiles along the mid-section (middle plane) of the square enclosure using different nanofluids and $Ra = 10^5$, $\varphi = 0.1$, $h = 0.5$ and $y_p = 0.5$. Due to buoyant flow inside the enclosure, the velocity shows a parabolic variation near the isothermal walls. The vertical velocity is not sensitive to the type of nanoparticles where three types of nanoparticles show similar vertical velocity. This is explained by looking at Eq. (8) where the Brinkman formula shows that the viscosity of the nanofluid is only sensitive to the volume fraction of particles and not influenced by the type of nanoparticles. However, the vertical velocity

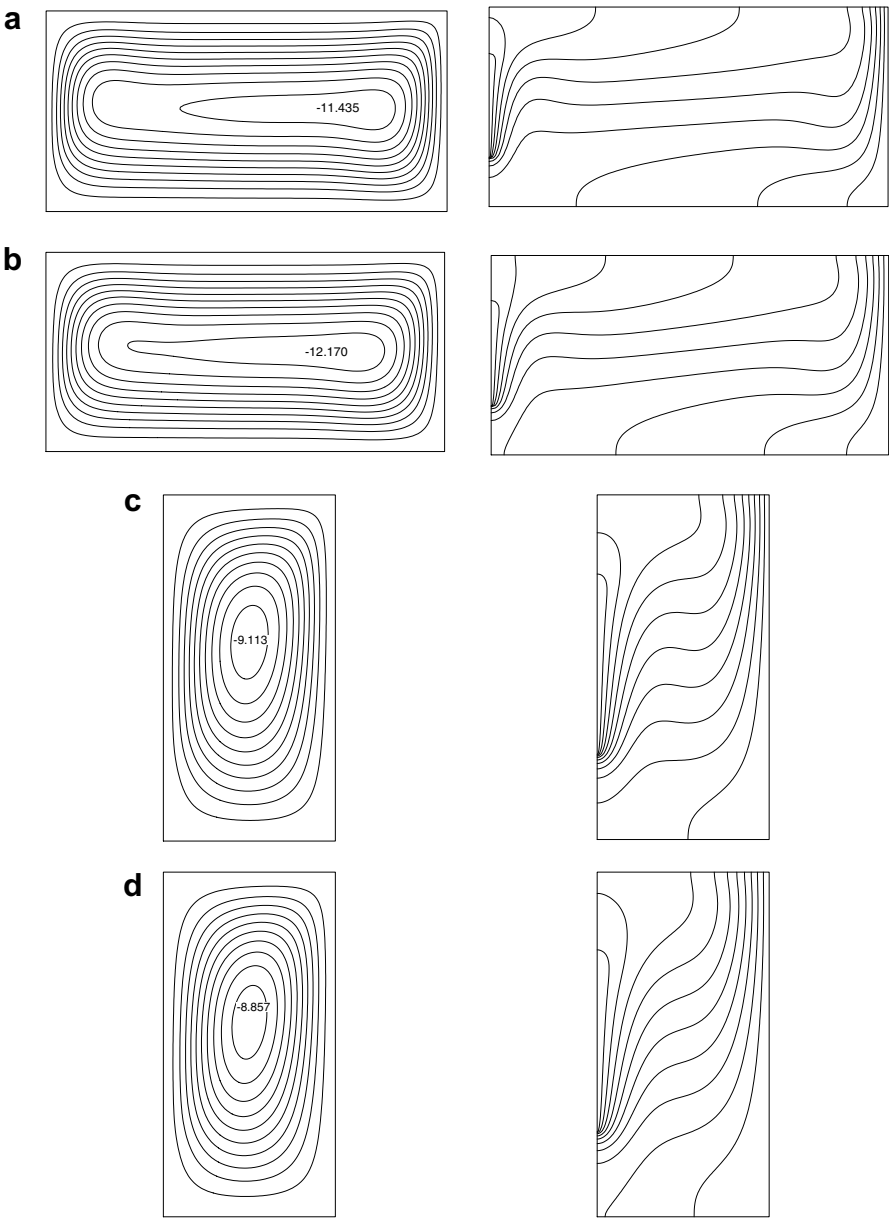

Fig. 9. Streamlines (on the left) and isotherms (on the right) for $Ra = 10^5$, $h = 0.5$, $y_p = 0.5$, (a) $A = 2$, $\varphi = 0.1$, (b) $A = 2$, $\varphi = 0.2$, (c) $A = 0.5$, $\varphi = 0.1$, (d) $A = 0.5$, $\varphi = 0.2$.

of nanofluid is lower than that of pure fluid at the hot side and higher at the cold side. It means that particle suspension affects the flow field. The flow velocity is almost zero around the center of the cavity. The profile also gives idea on flow rotation direction.

Using the same parameters given in Fig. 11, the variation of local Nusselt number is illustrated along the partial heater in Fig. 12 using different nanoparticles. Values of local Nusselt number have higher values at onset of heating and end point of the heater due to high temperature difference. As shown from the figure, almost U-shaped variation is obtained. Again, the highest local Nusselt number values were formed for Cu and the lowest one for pure fluid. Variation of local Nusselt number using different volume fraction of nanoparticles for different aspect ratios is given in Fig. 13 for $h = 0.5$, $y_p = 0.5$, $Ra = 10^5$ and Cu-water nanofluid. As shown from the figure, the heat transfer increases when increasing the volume fraction of nanoparticles. Thus, more particles are suspended and thermal conductivity of nanofluid increases. This result is supported by Khanafer et al. (2003). Also, the figure shows that as the aspect ratio increases the value of the Nusselt number decreases because of the decrease in temperature gradients. The three aspect ratios, as depicted in Fig. 13(a)–(c), show a similar trend in the variation of the Nusselt number. However, at the lower edge of the heater (i.e., $y = 0.25$) the value of the Nusselt number, for $A = 0.5$, is more sensitive to the presence of nanoparticles compared to $A = 2$. For example, at this edge, the enhancement in the Nusselt number when the volume fraction of nanoparticles is increased from 0 to 0.2, using $A = 0.5$, is approximately 40% whereas the enhancement is around 20% for $A = 2$. This finding is further supported in Fig. 14. The figure shows the variation of the mean Nusselt number using different aspect ratios. The enhancement in the mean Nusselt number when the volume fraction of nanoparticles is increased from 0 to 0.2, using $A = 0.5$, is approximately 26% whereas the enhancement is around 14% for $A = 2$. This tells that, for rectangular enclosures, the enhancement in heat transfer, due to the presence of nanoparticles, is more pronounced at low aspect ratio than at high aspect ratio.

Finally, the effect of dimensionless heater length (h'/H) on heat transfer is shown in Fig. 15 for $h = 0.5$, $y_p = 0.5$, $Ra = 10^5$ and $\varphi = 0.1$ using different nanofluids. The figure shows that heat transfer increases with heater size as expected due to increasing of heating surface. This graph is also supported by Chu et al. (1976) for pure fluid. An interesting result that the difference for heat transfer

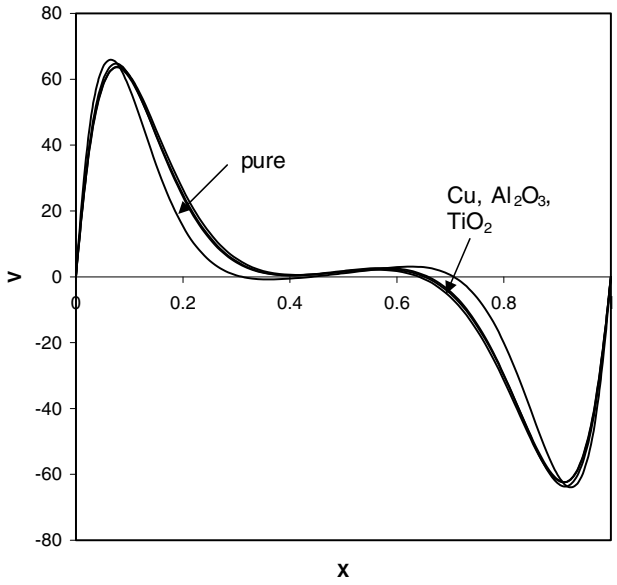

Fig. 11. Velocity profiles at the middle of the enclosure for different nano-particles $Ra = 10^5$, $Ra = 10^5$, $h = 0.5$, $A = 1$ and $y_p = 0.5$.

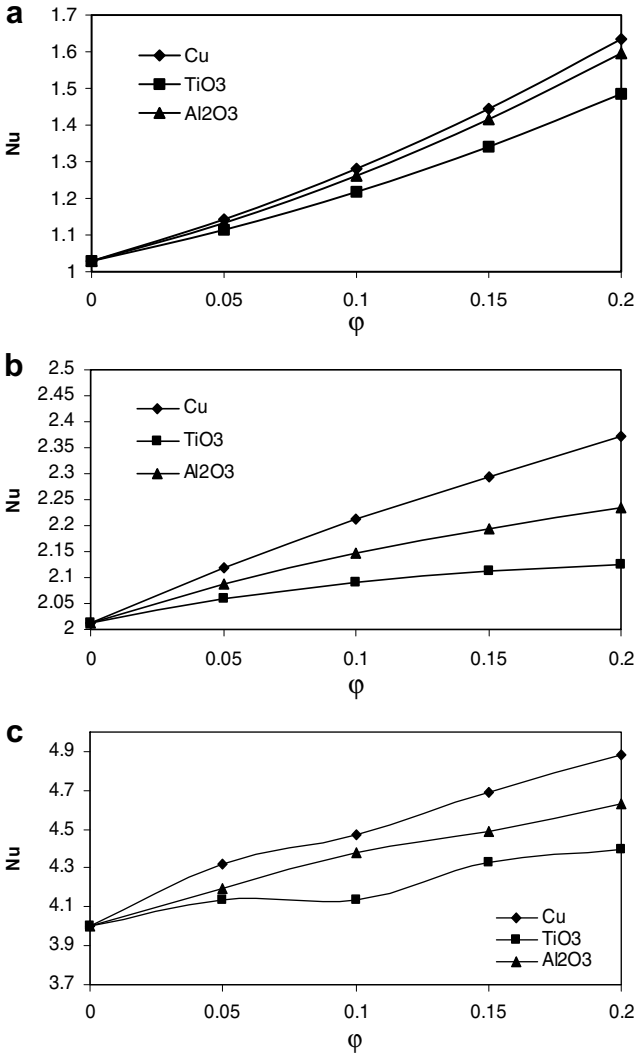

Fig. 10. Variation of mean Nusselt numbers with volume fraction for different nano-particles at $Ra = 10^5$, $h = 0.5$ and $y_p = 0.5$, (a) $Ra = 10^3$, (b) $Ra = 10^4$, (c) $Ra = 10^5$.

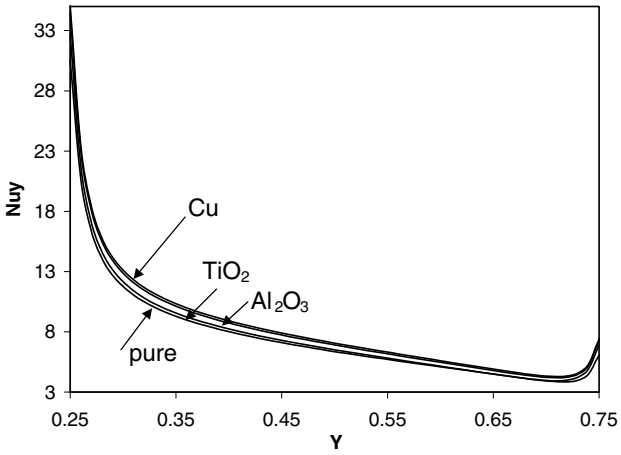

Fig. 12. Variation of local Nusselt number along the heated wall for different nanoparticles at $Ra = 10^5$, $h = 0.5$, $A = 1$ and $y_p = 0.5$.

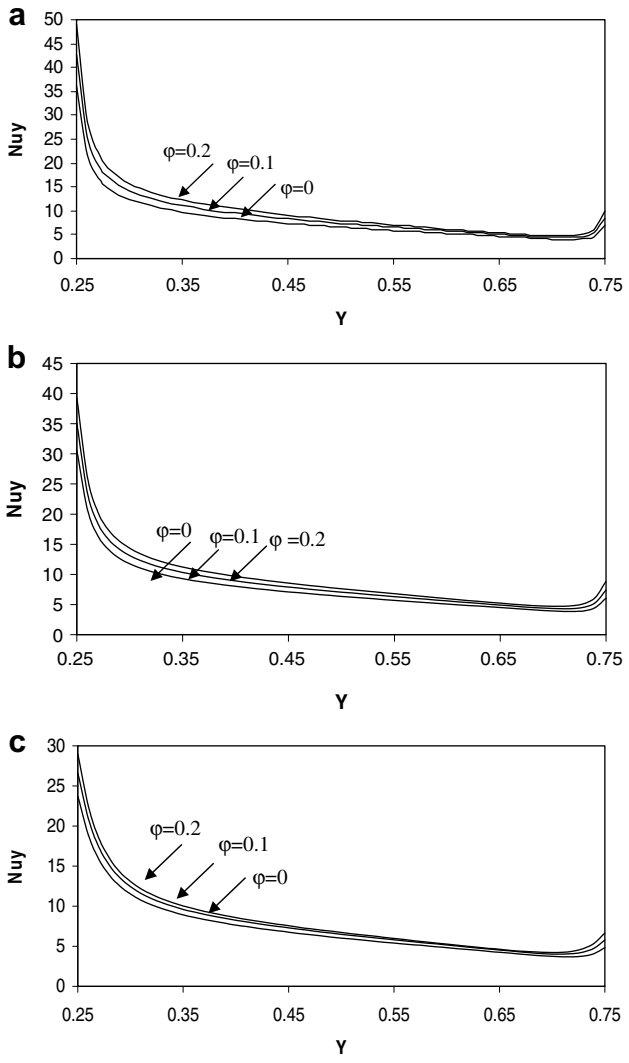

Fig. 13. Variation of local Nusselt number along the heated wall for different volume fraction at $Ra = 10^5$, $h = 0.5$ and $y_p = 0.5$ for Cu-water nanofluid, (a) $A = 0.5$, (b) $A = 1$, (c) $A = 2$.

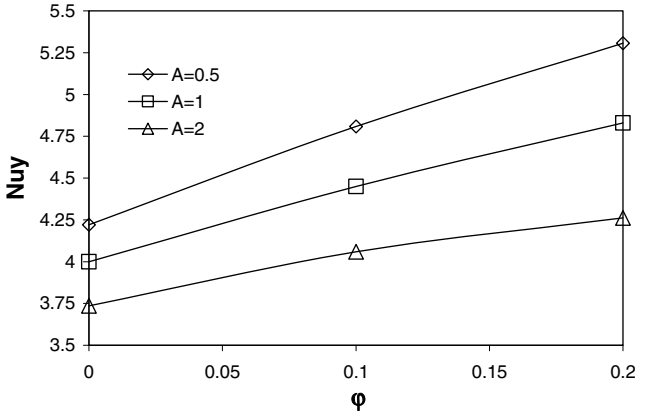

Fig. 14. Variation of mean Nusselt number for volume fraction for different aspect ratio, Cu-water nanofluid $h = 0.5$, $y_p = 0.5$, $Ra = 10^5$.

value becomes higher for higher heater size due convection mode of heat transfer becomes dominant. For lower heater size, values are almost equal for Cu and Al_2O_3. This figure also indicates that

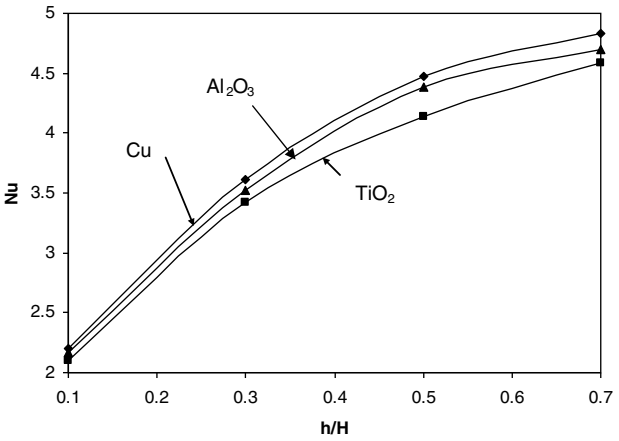

Fig. 15. Variation of mean Nusselt number for different length ratio of the heater and $h = 0.5$, $y_p = 0.5$, $Ra = 10^5$, $\varphi = 0.1$, $A = 1$, (b).

using of nanofluid enhances the natural convection heat transfer and Cu-nanofluid has the highest heat transfer enhancement.

6. Conclusions

A numerical study has been performed to investigate the effect of using different nanofluids on natural convection flow field and temperature distributions in partially heated square enclosure from the left vertical wall using MG model. Some important points can be drawn from the obtained results such as

(a) Both increasing the value of Rayleigh number and heater size enhances the heat transfer and flow strength keeping other parameters fixed.
(b) The type of nanofluid is a key factor for heat transfer enhancement. The highest values are obtained when using Cu nanoparticles.
(c) The difference in heat transfer, using different nanofluids, increases with increasing the value of volume fraction of nanoparticles.
(d) When increasing the heater size, the difference in heat transfer values is increased and depends mainly on the type of nanofluid used.
(e) For rectangular enclosures, the enhancement of heat transfer, due to the presence of nanoparticles, is more pronounced at low aspect ratio than at high aspect ratio.

In the future, the study can be extended for higher Rayleigh numbers, different types of nanofluids. An optimization study may be necessary for this study but it is not a goal of the present study.

References

Abu-Nada, E., 2008. Application of nanofluids for heat transfer enhancement of separated flows encountered in a backward facing step. Int. J. Heat Fluid Flow 29, 242–249.
Ahmed, G.R., Yovanovich, M.M., 1992. Numerical study of natural convection from discrete heat source in a vertical square enclosure. J. Thermophys. 6, 121–127.
Akbarinia, A., Behzadmehr, A., 2007. Numerical study of laminar mixed convection of a nanofluid in horizontal curved tubes. Appl. Therm. Eng. 27, 1327–1337.
Aydın, O., Yang, W.J., 2000. Natural convection in enclosures with localized heating from below and symmetrical cooling from sides. Int. J. Num. Meth. Heat Fluid Flow 10, 518–529.
Barakos, G., Mitsoulis, E., 1994. Natural convection flow in a square cavity revisited: laminar and turbulent models with wall functions. Int. J. Num. Meth. Fluids 18, 695–719.
Brinkman, H.C., 1952. The viscosity of concentrated suspensions and solutions. J. Chem. Phys. 20, 571–581.

Chao, P.K.B., Ozoe, H., Churchill, S.W., Lior, N., 1983. Laminar natural convection in an inclined rectangular box with lower surface half-heated and half-insulated. J. Heat Transfer 105, 425–432.

Choi, U.S. 1995. Enhancing thermal conductivity of fluids with nanoparticles, in: D.A. Siginer, H.P. Wang, (Eds.), Developments and applications of non-Newtonian flows, FED-vol. 231, 66, pp. 99–105.

Chu, H.H.S., Churchill, S.W., Patterson, C.V.S., 1976. The effect of heater size, location, aspect ratio, and boundary conditions on two-dimensional, laminar, natural convection in rectangular channels. ASME J. Heat Transfer, 194–201.

Daungthongsuk, W., Wongwises, S., 2007. A critical review of convective heat transfer nanofluids. Renew. Sustain. Energy Rev. 11, 797–817.

De Vahl Davis, G., 1983. Natural convection of air in a square cavity, a benchmark numerical solution. Int. J. Numer. Meth. Fluids 3, 249–264.

Farouk, B., Fusegi, T., 1989. Natural convection of a variable property gas in asymmetrically heated square cavities. J. Heat Transfer 3, 85–87.

Fusegi, T., Hyun, J.M., Kuwahara, K., Farouk, B., 1991. A numerical study of three-dimensional natural convection in a differentially heated cubical enclosure. Int. J. Heat Mass Transfer 34, 1543–1557.

Hasnaoui, M., Bilgen, E., Vasseur, P., 1992. Natural convection heat transfer in rectangular cavities partially heated from below. J. Thermophys. Heat Transfer 6, 255–264.

Hwang, K.S., Lee, Ji-Hwan, Jang, S.P., 2007. Buoyancy-driven heat transfer of water-based $Al_2 O_3$ nanofluids in a rectangular cavity. Int. J. Heat Mass Transfer 50, 4003–4010.

Ishihara, I., Fukui, T., Matsumoto, R., 2002. Natural convection in a vertical rectangular enclosure with symmetrically localized heating and cooling zones. Int. J. Heat Fluid Flow 23, 366–372.

Jang, S.P., Choi, S.U.S., 2004. Free convection in a rectangular cavity (Benard convection) with nanofluids. Proceedings of IMECE. Anaheim, California, USA.

Jou, R.Y., Tzeng, S.C., 2006. Numerical research of nature convective heat transfer enhancement filled with nanofluids in rectangular enclosures. Int. Comm. Heat Mass Transfer 33, 727–736.

Kang, H.U., Kim, S.H., Oh, J.M., 2006. Estimation of thermal conductivity of nanofluid using experimental effective particle volume. Exp. Heat Transfer 19, 181–191.

Khanafer, K., Vafai, K., Lightstone, M., 2003. Buoyancy-driven heat transfer enhancement in a two-dimensional enclosure utilizing nanofluids 46, 3639–3653.

Koca, A., Oztop, H.F., Varol, Y., 2007. The effects of Prandtl number on natural convection in triangular enclosures with localized heating from below. Int. Comm. Heat Mass Transfer 34, 511–519.

Krane, R.J., Jessee, J., 1983. Some detailed field measurements for a natural convection flow in a vertical square enclosure. Proceedings of the First ASME-JSME Thermal Engineering Joint Conference, vol. 1, 323-329.

Maiga, S.E.B., Palm, S.J., Nguyen, C.T., Roy, G., Galanis, N., 2005. Heat transfer enhancement by using nanofluids in forced convection flows. Int. J. Heat Fluid Flow 26, 530–546.

Markatos, N.C., Pericleous, K.A., 1984. Laminar and turbulent natural convection in an enclosed cavity. Int. J. Heat Mass Transfer 27, 772–775.

Nasr, K.B., Chouikh, R., Kerkeni, C., Guizani, A., 2006. Numerical study of the natural convection in cavity heated from the lower corner and cooled from the ceiling. Appl. Therm. Eng. 26, 772–775.

Ostrach, S., 1988. Natural convection in enclosures. J. Heat Transfer 110, 1175–1190.

Palm, S., Roy, G., Nguyen, C.T., 2006. Heat transfer enhancement with the use of nanofluids in a radial flow cooling systems considering temperature dependent properties. Appl. Therm. Eng. 26, 2209–2218.

Patankar, S.V., 1980. Numerical Heat Transfer and Fluid Flow. Hemisphere Publishing Corporation, Taylor and Francis Group, New York.

Polidori, G., Fohanno, S., Nguyen, C.T., 2007. A note on heat transfer modeling of Newtonian nanofluids in laminar free convection. Int. J. Therm. Sci 46, 739–744.

Putra, N., Roetzel, W., Das, S.K., 2003. Natural convection of nano-fluids. Heat Mass Transfer 39, 775–784.

Trisaksri, V., Wongwises, S., 2007. Critical review of heat transfer characteristics of nanofluids. Renew. Sustain. Energy Rev. 11, 512–523.

Turkoglu, H., Yucel, N., 1995. Effect of heater and cooler locations on natural convection in square cavities. Num. Heat Transfer Part A 27, 351–358.

Varol, Y., Koca, A., Oztop, H.F., 2006. Natural convection in a triangle enclosure with flush mounted heater on the wall. Int. Comm. Heat Mass Transfer 33, 951–958.

Versteeg, H.K., Malalasekera, W., 1995. An introduction to computational fluid dynamic: The finite volume method. John Wiley & Sons Inc, New York.

Wang, X-Q., Mujumdar, A.S., 2007. Heat transfer characteristics of nanofluids: a review. Int. J. Therm. Sci. 46, 1–19.

Wang, X.-Q., Mujumdar, A.S., Yap, C., 2006. Free convection heat transfer in horizontal and vertical rectangular cavities filled with nanofluids. International Heat Transfer Conference IHTC-13. 2006. Sydney, Australia.

Xuan, Y., Li, Q., 2000. Heat transfer enhancement of nanofluids. Int. J. Heat Fluid Flow 21, 58–64.

Further reading

Bourich, M., Hasnaoui, M., Amahmid, A., 2004. Double-diffusive natural convection in a porous enclosure partially heated from below and differentially salted. Int. J. Heat Fluid Flow 25, 1034–1046.